The Astrophysical Journal, 836:126 (8pp), 2017 February 10 doi:10.3847/1538-4357/836/1/126

Intermediate-mass Asymptotic Giant Branch Stars and Sources of ^{26}Al, ^{60}Fe, ^{107}Pd, and ^{182}Hf in the Solar System

G. J. Wasserburg[1,5], Amanda I. Karakas[2,3], and Maria Lugaro[2,4]
[1] Lunatic Asylum, California Institute of Technology, Pasadena, CA 91125, USA; gjw@gps.caltech.edu
[2] Monash Centre for Astrophysics, School of Physics and Astronomy, Monash University, VIC 3800, Australia
[3] Research School of Astronomy and Astrophysics, Australian National University, Canberra, ACT 2611, Australia
[4] Konkoly Observatory, Research Centre for Astronomy and Earth Sciences, Hungarian Academy of Sciences, H-1121 Budapest, Hungary
Received 2016 May 11; revised 2016 December 14; accepted 2016 December 15; published 2017 February 13

Abstract

We explore the possibility that the short-lived radionuclides ^{26}Al, ^{60}Fe, ^{107}Pd, and ^{182}Hf inferred to be present in the proto-solar cloud originated from 3–8 $M_\odot$ asymptotic giant branch (AGB) stars. Models of AGB stars with initial mass above 5 $M_\odot$ are prolific producers of ^{26}Al owing to hot bottom burning (HBB). In contrast, ^{60}Fe, ^{107}Pd, and ^{182}Hf are produced by neutron captures: ^{107}Pd and ^{182}Hf in models $\lesssim$5 $M_\odot$, and ^{60}Fe in models with higher mass. We mix stellar yields from solar-metallicity AGB models into a cloud of solar mass and composition to investigate whether it is possible to explain the abundances of the four radioactive nuclides at the Sun's birth using one single value of the mixing ratio between the AGB yields and the initial cloud material. We find that AGB stars that experience efficient HBB ($\geqslant$6 $M_\odot$) cannot provide a solution because they produce too little ^{182}Hf and ^{107}Pd relative to ^{26}Al and ^{60}Fe. Lower-mass AGB stars cannot provide a solution because they produce too little ^{26}Al relative to ^{107}Pd and ^{182}Hf. A self-consistent solution may be found for AGB stars with masses in between (4–5.5 $M_\odot$), provided that HBB is stronger than in our models and the ^{13}C(α, n)^{16}O neutron source is mildly activated. If stars of M $<$ 5.5 $M_\odot$ are the source of the radioactive nuclides, then some basis for their existence in proto-solar clouds needs to be explored, given that the stellar lifetimes are longer than the molecular cloud lifetimes.

Key words: nuclear reactions, nucleosynthesis, abundances – stars: AGB and post-AGB – ISM: abundances

1. Introduction

A self-consistent solution for the origin of the inventory of short-lived radioactive nuclides inferred to be present in the early solar system from meteoritic analysis is still missing. Proposed solutions include core-collapse supernovae (SNe; e.g., Takigawa et al. 2008; Pan et al. 2012) and low- and intermediate-mass asymptotic giant branch (AGB) stars (e.g., Wasserburg et al. 2006). Interestingly, a few isotopes (e.g., ^{53}Mn) can only be synthesized via explosive nucleosynthesis and are not produced in AGB stars. Some isotopes, such as ^{10}Be, ^{26}Al, ^{36}Cl, ^{41}Ca, and ^{53}Mn, can also be produced by spallation reactions induced by Galactic and solar cosmic rays (Gounelle et al. 2006). Notably, a stellar source is favored for ^{26}Al (e.g., Duprat & Tatischeff 2007; Fitoussi et al. 2008).

When considering the results from core-collapse SNe (SNe II) as possible contributors to the inventory of short-lived nuclei, we note the following: (1) the ratio ^{26}Al/^{27}Al in these sources is not very high, with production typically $\sim 5 \times 10^{-3}$ (Rauscher et al. 2002; Lugaro et al. 2014); (2) the ratio of ^{60}Fe/^{56}Fe predicted is $\sim 2.4 \times 10^{-3}$; and (3) ^{53}Mn is abundantly produced, where the ratio ^{53}Mn/^{55}Mn $\approx$ 0.15. This is not very different from the earlier results of Woosley & Weaver (1995). As noted in Wasserburg et al. (2006), these results require dilution factors of $\approx 10^{-2}$ to 10^{-4} between the SN II yields and the proto-solar cloud in order to account for the proto-solar ratios of ^{26}Al/^{27}Al, ^{60}Fe/^{56}Fe, and ^{53}Mn/^{55}Mn in the early solar system (see, e.g., Figure S1 of Lugaro et al. 2014). It follows that SNe II cannot explain the ^{26}Al inventory, nor can they significantly contribute to the Fe and Mn isotopes.

The emphasis here is on AGB production of the four short-lived nuclei with mean lives less than about 10^7 yr. The list of isotopes includes ^{26}Al (with a mean life $\overline{\tau}_{26}$ = 1.03 Myr), ^{60}Fe ($\overline{\tau}_{60}$ = 3.75 Myr), ^{107}Pd ($\overline{\tau}_{107}$ = 9.38 Myr), and ^{182}Hf ($\overline{\tau}_{182}$ = 12.8 Myr). These isotopes can be produced in AGB stars by proton captures (^{26}Al) or by neutron captures (^{60}Fe, ^{107}Pd, ^{182}Hf).

The isotope ^{26}Al is a by-product of the MgAl chain operating in hydrogen-burning environments (e.g., Arnould et al. 1999). Intermediate-mass AGB stars that experience hot bottom burning (HBB) can produce ^{26}Al in copious quantities (Mowlavi & Meynet 2000; Karakas & Lattanzio 2003; Izzard et al. 2007; Ventura et al. 2011). HBB occurs when the temperature at the base of the convective envelope exceeds 50×10^6 K, hot enough for proton-capture nucleosynthesis (Bloecker & Schoenberner 1991; Boothroyd & Sackmann 1992; Lattanzio 1992). HBB changes the surface composition because the whole convective envelope is constantly mixed into the hot region, with a mixing time of the order of $\approx$1 yr. The minimum stellar mass for HBB to occur depends on the initial composition and the input physics used in the calculations (Ventura & D'Antona 2005a, 2005b). For solar metallicity, which we define here to be Z = 0.014 adopting the solar composition of Asplund et al. (2009), the minimum mass for HBB in our models is 4.5 $M_\odot$ (Karakas 2014). Note that ^{26}Al is easily destroyed by (n, α) and (n, p) reactions, so it cannot be produced by neutron captures.

Charged particle reactions on isotopes heavier than Si are unlikely to occur at AGB temperatures (Iliadis et al. 2016). For this reason the heavier radioactive nuclides ^{60}Fe, ^{107}Pd, and ^{182}Hf can be synthesized in AGB stars only by neutron captures occurring in the He-rich shell. While ^{60}Fe is predominantly

[5] *Deceased.*

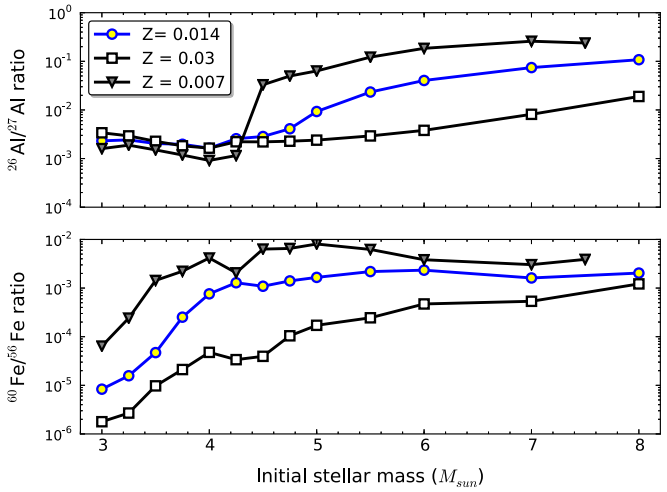

Figure 1. Predicted isotopic ratios for ^{26}Al/^{27}Al and ^{60}Fe/^{56}Fe (ratios are shown by number) as a function of initial stellar mass $M \geqslant 3\,M_{\odot}$, for the three metallicities included in Karakas & Lugaro (2016). The ratios are calculated from the surface composition after the final thermal pulse. These are almost the same as the ratios calculated from the stellar yields because the yields are determined when most of the mass is lost from the star and this is near the tip of the AGB.

produced by neutron captures occurring in massive stars (Limongi & Chieffi 2006), it can also be made in intermediate-mass AGB stars (Trigo-Rodríguez et al. 2009; Lugaro & Karakas 2008; Lugaro et al. 2012). For the isotopes heavier than Fe, ^{107}Pd and ^{182}Hf, the main processes of neutron-capture nucleosynthesis are the *slow* neutron-capture process and the *rapid* neutron-capture process (the *s*- and the *r*-process, respectively; Meyer 1994; Käppeler et al. 2011). The *s*-process has been confirmed observationally to operate in low-mass AGB stars (Gallino et al. 1998; Abia et al. 2002) and is a possible source of both ^{107}Pd and ^{182}Hf (Lugaro et al. 2014).

Previously, the *r* process was considered the dominant site of ^{182}Hf in the Galaxy; however, Lugaro et al. (2014) pointed out that there is a good basis for the production of ^{182}Hf in AGB stars since the lifetime of the precursor nucleus ^{181}Hf in stellar environments is not too short: the nuclear structure of the ^{181}Hf nucleus used by Takahashi & Yokoi (1987) was the basis of the decrease of the half-life of ^{181}Hf from ≃42 days to ≃3 hr in stellar interiors and the attribution of the origin of ^{182}Hf to the *r*-process. However, due to new data on the states of ^{181}Hf by Bondarenko et al. (2002), the decrease in the half-life is now minimal. This permits the inclusion of ^{182}Hf in the inventory of AGB products and is not the result of multiple *r*-process events as inferred by Wasserburg et al. (1994) from comparison with the abundance of ^{129}I ($\overline{\tau}_{129} = 22.6$ Myr), which can only be produced by the *r*-process. In the report by Lugaro et al. (2014), updated and revised models are presented together with an extensive discussion of the ratios ^{107}Pd/^{108}Pd and ^{182}Hf/^{180}Hf for a wide range of stellar masses. A time of 10–30 Myr from the last AGB *s*-process event was obtained to match the ^{107}Pd/^{108}Pd and ^{182}Hf/^{180}Hf ratios in the early solar system, during which the ^{26}Al/^{27}Al produced by this intermediate-mass star would have completely decayed. A separate ^{26}Al source was assumed, and no discussion was given in relation to the other short-lived isotope ^{60}Fe. Here, we follow in detail the possible implications of the important revision on the AGB production of ^{182}Hf to the scenario of an AGB source for some short-lived nuclei.

We present a detailed analysis of the possibility that the isotopic shifts in the solar system for the four radioactive nuclei considered here were due to injection of freshly synthesized radioactive nuclei, using the latest set of AGB star yields from Karakas & Lugaro (2016). We begin with a brief overview of AGB nucleosynthesis relevant to the production of the short-lived nuclides found in the early solar system (Section 2). In Section 3 we consider the extent to which any self-consistent solution for the estimated solar inventory can be found for the relative masses of the fresh stellar ejecta to the mass of the proto-solar cloud. A key to the dilution factor is the abundance ratio of short-lived nuclei relative to stable isotopes of the same element in the AGB ejecta and the ratios at some reference time in the early solar system. There are reliable data estimating the abundance ratios at some times in the early solar system for ^{26}Al/^{27}Al (which we further discuss in Appendix A), ^{107}Pd/^{108}Pd, and ^{182}Hf/^{180}Hf, but not for ^{60}Fe/^{56}Fe, as we discuss in Appendix B. For completeness, in Section 4 we discuss the potential issues with current AGB models and their impact on our results. In Section 5 we present our conclusions.

2. AGB Star Nucleosynthesis

Low- and intermediate-mass stars cover a range in mass of 0.8–8 $M_{\odot}$ for solar metallicity (see Figure 1 from Karakas & Lattanzio 2014). Nucleosynthesis during the AGB is driven by He-shell instabilities. These thermal pulses (TPs) may result in mixing between the H-exhausted core and the envelope; this is known as third dredge-up (TDU), which alters the composition of the envelope by bringing the products of He-shell burning and the elements produced by the *s*-process to the stellar surface. For a review of AGB stars and their associated nucleosynthesis we refer to Busso et al. (1999), Herwig (2005), and Karakas & Lattanzio (2014).

Low-mass AGB stars with initial masses $M \lesssim 4\,M_{\odot}$ have their surface compositions altered primarily by TDU, which results in enrichments in carbon, nitrogen, fluorine, and *s*-process elements (Busso et al. 2001; Abia et al. 2002; Karakas & Lattanzio 2007; Karakas 2010; Cristallo et al. 2011, 2015; Karakas & Lugaro 2016). In comparison, intermediate-mass AGB stars with initial masses $M \gtrsim 4\,M_{\odot}$ experience the second dredge-up during the early AGB and HBB during the thermally pulsing AGB (e.g., Ventura et al. 2013). The surface chemistry of intermediate-mass stars therefore shows the results of proton-capture nucleosynthesis, with some contribution from the He shell depending on the amount of TDU (Karakas et al. 2012; Ventura et al. 2013; Fishlock et al. 2014; Cristallo et al. 2015).

The AGB models we are using in this study are from Karakas & Lugaro (2016). In brief, we use the stellar structure from detailed stellar evolution calculations as input into a post-processing code that calculates the abundance changes due to nuclear reactions and mixing. We use 328 isotopes from the neutron to polonium and roughly 2500 reactions from the JINA database as of 2012 May. We refer to Karakas & Lugaro (2016) for further details on the numerical method and the input physics used in the calculations.

In Karakas & Lugaro (2016) we compare our results to other AGB models in the literature, including the models of Cristallo et al. (2015) and Pignatari et al. (2016), while Ventura et al. (2015) compared intermediate-mass AGB models with HBB from Karakas (2010) and Ventura et al. (2013). The summary is that the low-mass ($<4\,M_{\odot}$) models from Cristallo et al. (2015) are comparable in terms of their nucleosynthesis to the

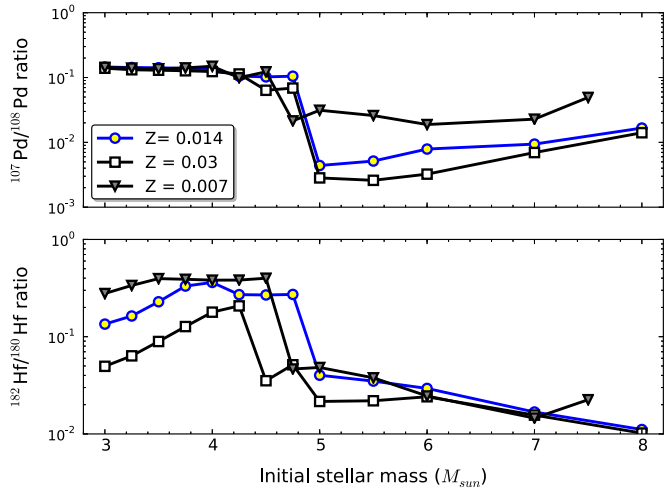

Figure 2. Same as Figure 1, except for the ^{107}Pd/^{108}Pd and ^{182}Hf/^{180}Hf ratios.

low-mass models from Karakas & Lugaro (2016), especially for heavy elements produced by the *s*-process. In contrast, the higher-mass models of Karakas & Lugaro (2016) experience HBB at much higher temperature at a given mass compared to the models by Cristallo et al. (2015), and they also show much deeper TDU. Models by Pignatari et al. (2016) are comparable to the models by Karakas & Lugaro (2016) for intermediate masses, in terms of the depth of TDU and HBB temperatures (see also models by Weiss & Ferguson 2009; Marigo et al. 2013). Models by Ventura et al. (2013) show even higher HBB temperatures than those by Karakas & Lugaro (2016) for the same mass and composition but have much less TDU. The implications of these differences for the radio nuclei discussed here and our results are detailed in Section 4.

In Figure 1 we show the predicted ^{26}Al/^{27}Al and ^{60}Fe/^{56}Fe ratios for the models with initial mass $M \geqslant 3\,M_{\odot}$ using data from Karakas & Lugaro (2016). The initial ratios are zero. From this figure we can see that the major difference between low-mass (1.5–4 $M_{\odot}$) AGB stars and intermediate-mass stars is the production of ^{26}Al. HBB results in copious ^{26}Al production, with ratios $\approx$0.1, in contrast to the situation for C-rich lower-mass stars, which generally have ratios $<10^{-2}$ (see, e.g., van Raai et al. 2008).

The minimum ^{26}Al/^{27}Al ratio required in the envelope of an AGB star is $\approx 2 \times 10^{-2}$ in order to produce enough ^{26}Al to explain the amount inferred to be present in the early solar system (Wasserburg et al. 2006). From Figure 1 we see that only models with masses above 4.5 $M_{\odot}$ satisfy this criterion. If we are to consider a lower-mass star of $\approx$3 $M_{\odot}$ as being responsible for the inventory of radioactive nuclides, we need to invoke some form of slow nonconvective transport mechanism to explain the ^{26}Al. Such deep mixing is invoked to occur in the envelopes of low-mass ($\lesssim$2 $M_{\odot}$) red giant branch stars (e.g., Gilroy 1989; Gilroy & Brown 1991). Evidence comes from observations of lower ^{12}C/^{13}C and C/N ratios compared to theoretical models (Charbonnel 1994; Boothroyd et al. 1995; Nollett et al. 2003; Charbonnel & Zahn 2007; Eggleton et al. 2008). This process results in proton captures producing ^{13}C and ^{14}N. If it occurs also in AGB stars and if deeper layers are reached where the temperature is higher, then ^{26}Al and ^{17}O can also be produced (e.g., Palmerini et al. 2011).

The mechanism responsible for the deep mixing is not known, although in recent years parameterized versions of thermohaline mixing have been found to work, at least for the C and N isotopes in red giant branch stars (e.g., Angelou et al. 2012). Note that observational evidence for deep mixing for elements heavier than nitrogen is not well established from stellar spectra. Evidence for heavier isotopes instead comes from presolar grains, which are believed to have condensed in the atmospheres of evolved stars (see the extensive report by Zinner 2014, pp. 181–213). However, no a priori prediction of the ^{26}Al yield for low-mass AGB stars is possible to be used for dilution calculations. Instead, the degree of deep mixing required to give the observed ^{26}Al/^{27}Al ratio is calculated to match the other observations. In contrast, for models with HBB the ^{26}Al yields are directly calculated for a stellar model. This is a direct result of the elevated temperatures in these more massive systems.

2.1. The s-Process in AGB Stars

The isotopes ^{60}Fe, ^{107}Pd, and ^{182}Hf are produced exclusively by neutron-capture reactions. The main neutron source in low-mass AGB stars of $M \lesssim 4\,M_{\odot}$ is the ^{13}C(α, n)^{16}O reaction (Abia et al. 2001, 2002). CN cycling does not leave enough ^{13}C nuclei in the He intershell to produce enough *s*-process elements to match observations (Busso et al. 2001). The solution to this problem is to assume that some partial mixing occurs between the H-rich envelope and the intershell at the deepest extent of each TDU. The protons are captured by ^{12}C to produce a region rich in ^{13}C, known as a ^{13}C "pocket." The inclusion of ^{13}C pockets in theoretical calculations of AGB stars is one of the most significant uncertainties affecting predictions of the *s*-process (see discussions in Busso et al. 1999; Herwig 2005; Käppeler et al. 2011; Karakas & Lattanzio 2014).

The details of how we include ^{13}C pockets in our models are discussed in Karakas & Lugaro (2016). Briefly, at the deepest extent of each TDU episode we include protons in the top layers of the He-rich intershell region. Those protons are quickly captured by the abundant ^{12}C and converted into ^{13}C and ^{14}N by CN cycle reactions. Fishlock et al. (2014) compared the shape and size of the ^{13}C pockets from this method to those calculated more self-consistently by Cristallo et al. (2011) and found good agreement. For models $M \leqslant 3\,M_{\odot}$ we include protons down to a depth in mass in the He intershell of $2 \times 10^{-3}\,M_{\odot}$, which results in a ^{13}C pocket that is $\approx$1/10 of the mass of the He intershell.

In intermediate-mass stars the He intershell becomes hot enough to activate the ^{22}Ne(α, n)^{25}Mg reaction inside the TP. For masses in the transition between mild and strong HBB (4–5 $M_{\odot}$ for solar metallicity) there will be a contribution from both the ^{13}C and the ^{22}Ne neutron source. In intermediate-mass AGB stars with strong HBB ($M \gtrsim 5\,M_{\odot}$), evidence suggests that ^{13}C pockets do not form and the *s*-process is the result of the ^{22}Ne reaction (Goriely & Siess 2004; García-Hernández et al. 2013). In the $Z = 0.014$ models from Karakas & Lugaro (2016) we include ^{13}C pockets in models $<5\,M_{\odot}$, with the size of the ^{13}C pocket decreasing as a function of increasing stellar mass. We also test the case of including ^{13}C pockets in the 5 $M_{\odot}$ model. Because the intershell region is smaller by roughly an order of magnitude in this case, we reduce the mass over which we mix protons by a similar factor to $1 \times 10^{-4}\,M_{\odot}$ (e.g., as discussed in Karakas & Lugaro 2016).

Table 1
Isotopic Ratios in the Early Solar System at the CAI ($R^0_{i,j}$) and Cooling ($R^{\tau P2}_{i,j}$) Reference Times

Isotope	$\overline{\tau}_i$ (yr^{-1})	$R^0_{i,j}$	$R^{\tau P2}_{i,j}$
^{26}Al	1.03×10^6	5.5×10^{-5}	...
^{60}Fe	3.75×10^6	$<10^{-6}$	$<2 \times 10^{-6}$
^{107}Pd	9.38×10^6	$2.4 \times 10^{-5} \exp(\tau_{P2}/\overline{\tau}_i)$	2.4×10^{-5}
^{182}Hf[a]	12.8×10^6	9.72×10^{-5}	...

Note.
[a] Using data from Burkhardt et al. (2008). Note that Kruijer et al. (2014a) give $(1.018 \pm 0.043) \times 10^{-4}$.

The predicted ratios from stellar models are shown in Figures 1 and 2. The ^{60}Fe/^{56}Fe ratio follows ^{26}Al/^{27}Al, where intermediate-mass AGB stars over 5 $M_\odot$ produce the most ^{26}Al and ^{60}Fe. The reason is that to produce ^{60}Fe, it is necessary to bypass the branching point at ^{59}Fe ($\overline{\tau}_{59} = 64$ days), which requires neutron densities above $\sim 10^9$ n cm^{-3}. Such high neutron densities can only be produced inside TPs when the temperatures and densities are high enough to activate the ^{22}Ne neutron source, above 300×10^6 K. This is achieved inside models of intermediate mass.

In contrast, the ratios of ^{107}Pd/^{108}Pd and ^{182}Hf/^{180}Hf are relatively flat for models $<5\,M_\odot$ but drop by an order of magnitude in the more massive AGB stars. The reason is that significant amounts of these isotopes can only be synthesized if the neutron exposure is relatively high, which is when the ^{13}C pocket is included in the low-mass models, which allows for activation of the ^{13}C(α, n)^{16}O neutron source reaction. Hence, high absolute abundances in the He-rich region (and consequently a strong signature at the stellar surface) are possible only when the ^{13}C pocket is included. The isotope ^{182}Hf is further dependent on the branching point at ^{181}Hf, which has a similar mean life to ^{59}Fe; hence, its abundance reaches a maximum in models of $\simeq 4\,M_\odot$, where both the ^{13}C and ^{22}Ne neutron sources are activated. As noted above, in intermediate-mass AGB stars the mass of the He intershell drops by an order of magnitude. While these models are predicted to experience many more TPs than their lower-mass counterparts (e.g., Doherty et al. 2014), the total amount of dredged-up material is lower than or similar to their lower-mass counterparts (see Figure 1 from Karakas & Lugaro 2016).

3. The Mixing Model

The mixing model used here represents the addition of freshly synthesized nuclei to the solar nebula in the framework of a molecular cloud with a variety of stars and the consideration of the times of formation of objects in the early solar system. Relative to some time (τ_0) in the very early solar system, debris from an AGB star that underwent major mass loss at a (negative) time $\tau_{\rm AGB}$ is mixed with 1 $M_\odot$ of matter of solar composition with the mixing factor $F = M_{\rm AGB}/(M_{\rm AGB} + M_\odot) \approx M_{\rm AGB}/M_\odot$. Here $M_{\rm AGB}$ represents the debris from the AGB star and is a small fraction of the total mass lost from the AGB star's envelope. We use exactly the same formalism described in detail in Wasserburg et al. (2006; see their Equations (6) and (7)). For each isotope pair i (unstable), j (stable) listed in Table 1 we define $F_{i,j}$ as the mixing factor derived by imposing that the mixing produces the ratios $R_{i,j}$ observed in the early solar system:

$$F_{i,j} = \frac{R_{i,j}}{R^{\rm AGB}_{i,j} \times PF^{\rm AGB}_j},$$

where $R^{\rm AGB}_{i,j}$ is the isotopic ratio from the AGB stellar yields and $PF^{\rm AGB}_j$ is the AGB production factor of the stable isotope j, relative to its initial solar abundance. Clearly, a self-consistent solution for all four isotope pairs considered here needs to produce the same value for the four $F_{i,j} = F$.

Table 2
Ratios by Number in the Net Ejecta from Karakas & Lugaro (2016) for Models without ^{13}C Pockets

Isotope	5 $M_\odot$	6 $M_\odot$	7 $M_\odot$	8 $M_\odot$
^{26}Al/^{27}Al	9.47×10^{-3}	4.24×10^{-2}	7.29×10^{-2}	8.85×10^{-2}
^{60}Fe/^{56}Fe	9.55×10^{-4}	1.14×10^{-3}	7.11×10^{-4}	7.45×10^{-4}
^{107}Pd/^{108}Pd	3.42×10^{-3}	5.37×10^{-3}	7.67×10^{-3}	1.19×10^{-2}
^{182}Hf/^{180}Hf	3.52×10^{-2}	2.24×10^{-2}	1.11×10^{-2}	5.47×10^{-3}

Table 3
Ratios by Number in the Net Ejecta from Karakas & Lugaro (2016) for Models with ^{13}C Pockets

Isotope	3 $M_\odot$[a]	5 $M_\odot$[b]
^{26}Al/^{27}Al	2.28×10^{-3}	9.50×10^{-3}
^{60}Fe/^{56}Fe	6.74×10^{-6}	9.12×10^{-4}
^{107}Pd/^{108}Pd	1.45×10^{-1}	9.97×10^{-2}
^{182}Hf/^{180}Hf	1.25×10^{-1}	2.47×10^{-1}

Notes.
[a] For the 3 $M_\odot$ model with a standard ^{13}C pocket; see details in Karakas & Lugaro (2016).
[b] Using the one calculation of a 5 $M_\odot$ model with a ^{13}C pocket from Karakas & Lugaro (2016).

3.1. Input to the Model

The reference data used for all our calculations are given in Tables 1–3. We use the stellar model results of Karakas & Lugaro (2016) for $Z = 0.014$ and proto-solar abundances from Asplund et al. (2009). Table 1 shows the mean lifetime of species i, $\overline{\tau}_i$, given in years, for the ratios ^{26}Al/^{27}Al, ^{107}Pd/^{108}Pd, and ^{182}Hf/^{180}Hf at the calcium-aluminum (CAI) reference time with ^{26}Al/^{27}Al $= 5.5 \times 10^{-5}$ in the early solar system. The ratio of ^{60}Fe/^{56}Fe is further discussed in Appendix B. Tables 2 and 3 show the predicted ratios of ^{26}Al/^{27}Al, ^{60}Fe/^{56}Fe, ^{107}Pd/^{108}Pd, and ^{182}Hf/^{180}Hf from the AGB yields calculated by Karakas & Lugaro (2016). Table 2 shows the predictions for intermediate-mass AGB models that do not include a ^{13}C pocket. Table 3 shows predictions for two masses (3 $M_\odot$ and 5 $M_\odot$), which include ^{13}C pockets.

One further complication is related to the timescale of the formation of the objects from whose analysis the initial abundance in the solar system is derived. At time τ_0, CAIs are formed; at later times ($\tau_{\rm P1}$) proto-planet formation occurs with a variety of types of chemical fractionation (Fe–Ni, FeS, silicate separation from bulk material with major chemical fractionation); this is followed at later times ($\tau_{\rm P2}$) by cooling of planetary material and the freezing in of chemical fractionation and diffusion. Some of the data on meteoritic samples are made on different chemical phases in a single object to produce an

Table 4
Mixing Ratios $F_{i,j}$ for the Models without ^{13}C Pockets

Mass	$F_{26,27}$	$F_{107,108}$	$F_{182,180}$
5 $M_\odot$	5.8×10^{-3}	$7.0 \times 10^{-3}\exp(\tau_{P2}/\overline{\tau}_i)$	3.0×10^{-3}
6 $M_\odot$	1.3×10^{-3}	$4.5 \times 10^{-3}\exp(\tau_{P2}/\overline{\tau}_i)$	4.3×10^{-3}
7 $M_\odot$	7.5×10^{-4}	$3.1 \times 10^{-3}\exp(\tau_{P2}/\overline{\tau}_i)$	8.8×10^{-3}
8 $M_\odot$	6.2×10^{-4}	$2.0 \times 10^{-3}\exp(\tau_{P2}/\overline{\tau}_i)$	1.8×10^{-2}

Table 5
Mixing Ratios $F_{i,j}$ for Models with ^{13}C Pockets

Mass	$F_{26,27}$	$F_{107,108}$	$F_{182,180}$
3 $M_\odot$	2.4×10^{-2}	$1.74 \times 10^{-4}\exp(\tau_{P2}/\overline{\tau}_i)$	7.8×10^{-4}
5 $M_\odot$	5.8×10^{-3}	$2.4 \times 10^{-4}\exp(\tau_{P2}/\overline{\tau}_i)$	3.9×10^{-4}

Table 6
$R^0_{60,56}$ Calculated from $F_{182,180}$

Mass	$R^0_{60,56}$
Models Calculated with a ^{13}C Pocket	
3 $M_\odot$	5.3×10^{-9}
5 $M_\odot$	3.6×10^{-7}
Models Calculated without ^{13}C Pockets	
5 $M_\odot$	2.9×10^{-6}
6 $M_\odot$	4.9×10^{-6}
7 $M_\odot$	6.3×10^{-6}
8 $M_\odot$	1.3×10^{-5}

internal isochron. The time this represents is when the object cooled (τ_{P2}), not necessarily when it formed (τ_{P1}), and gives the ratio (of, say, ^{107}Pd/^{108}Pd) in that object at τ_{P2}. CAIs typically contain clear evidence of ^{26}Al with a maximum value of ^{26}Al/^{27}Al $= 5.5 \times 10^{-5}$. These CAIs are used to represent the initial reference time (τ_0). ^{26}Al is used because of the short mean life ($\overline{\tau}_{26Al} = 1.03 \times 10^6$ yr) and its widespread nature in CAIs. CAIs are surmised to be condensates from a mass of hot solar nebular gas. The actual mechanism that produced CAIs is not in fact known, nor do we know that they were produced at one time or place or at what stage of growth the Sun had attained. It is known that CAI formation took place over an extended time ($>10^5$ yr; Hsu et al. 2000). More discussion can be found in Appendix A.

The key short-lived isotopes discussed here are ^{26}Al, ^{60}Fe, ^{182}Hf, and ^{107}Pd. Of these, only the values at the CAI formation time for ^{26}Al and ^{182}Hf are well determined. The thorough and extensive studies by Burkhardt et al. (2008) and Kruijer et al. (2013) have established internal isochrons for Hf-W on CAIs. This gives a direct comparison for these nuclei of refractory elements at what is plausibly the same time. An insightful and thorough investigation of ^{182}Hf/^{180}Hf in bulk FeNi meteorites was carried out by Kruijer et al. (2014a), corrected for cosmic-ray effects using ^{196}Pt as a monitor. These workers established initial values of ^{182}Hf/^{180}Hf for Fe–Ni segregation from silicates. These results are not internal isochrons but represent the times when bulk Hf-W chemical fractionation took place between metal and silicate masses in parent planets. These workers find that there was a rather short time between τ_{P1} and τ_{CAI} (several million years; see Kruijer et al. 2014b, their supplemental data). In contrast, for ^{107}Pd we know from internal isochrons for three meteorites (Gibeon, Duchesne, Muonionalusta) that ^{107}Pd/^{108}Pd $= 2.4 \times 10^{-5}$ (Chen & Wasserburg 1996; Horan et al. 2012), and see Matthes et al. (2015) for the most precise value for Muonionalusta. The ^{107}Pd/^{108}Pd ratio for these samples is the value when the diffusion process stopped between the coexisting phases in these objects. It is some τ_{P2}. It is not the same time as that for bulk Fe–Ni–silicate segregation. Matthes et al. (2015) have the most precise and thorough analysis and discussion of the ^{107}Pd-^{107}Ag system.

3.2. Results

To gain some insight into the problem of self-consistent models, we first consider mixing ratios for ^{26}Al/^{27}Al and ^{182}Hf/^{180}Hf (see Tables 4–5). Table 4 shows the values of $F_{i,j}$ for the three isotopic pairs for which early solar system ratios have been determined, using the reference values at CAI time given in Table 1 and the ratios in the ejecta (Tables 2 and 3) for different stellar masses. It can be seen that the mixing ratio is very high for ^{26}Al at lower masses and then decreases drastically, reflecting the much higher temperatures accessible in more massive stars. In contrast, ^{182}Hf produced by neutron captures gives low $F_{182,180}$ values at lower masses and then rapidly increases to very high mixing ratios. The only apparent solution for this couplet is at $\approx$5.5 $M_\odot$. Higher mass values are excluded for this isotopic pair. For ^{107}Pd, it is seen that $F_{107,108}$ always exceeds $F_{26,27}$. If we seek to match only ^{107}Pd and ^{182}Hf, we find that τ_{P2} should be $\approx 9 \times 10^6$ yr for the 7 $M_\odot$ case. This value is reasonable. For the 8 $M_\odot$ case τ_{P2} is $\approx 18 \times 10^6$ yr instead. For these high masses all solutions that can match the initial solar values require very high mixing ratios ($>4 \times 10^{-3}$) to obtain the right amounts of ^{182}Hf and ^{107}Pd. This then would also require the ^{26}Al that is co-produced to have significantly decayed. This requires consideration of an AGB event that precedes the initial formation of the solar system by several million years ($\tau_{AGB} \approx 3 \times 10^6$ yr).

Now, we consider the ratio of ^{60}Fe/^{56}Fe that would occur for intermediate-mass stars if the mixing ratio for ^{182}Hf/^{180}Hf were used for ^{60}Fe. We see from Table 6 that for all cases above about 5 $M_\odot$ the ^{60}Fe/^{56}Fe ratio to be expected at CAI time is above 10^{-6}. While the abundance of ^{60}Fe is not well established (see Appendix B), it is clear that ^{60}Fe/^{56}Fe $<10^{-6}$ is the upper bound possible at CAI time from all the data available. It follows that any attempt to attribute the origin of both ^{182}Hf and ^{26}Al to an intermediate-mass star is excluded from consideration of ^{60}Fe. We note that Lugaro et al. (2014) (see their Figure S1) also found for the 6 $M_\odot$ case that possible self-consistent solutions with $F \sim 0.005$ would have much too high a value for ^{60}Fe/^{56}Fe.

For the 3 $M_\odot$ case (Table 5) we see that the ^{182}Hf and ^{107}Pd are essentially concordant if $\tau_{P2} = 14$ Myr. It is evident that ^{26}Al is grossly underproduced by a factor of 31. This is typical of all low-mass AGB stars, as has long been recognized. For a 3 $M_\odot$ star to produce enough ^{26}Al and match ^{182}Hf would require ^{26}Al/^{27}Al $\approx 2 \times 10^{-2}$ in the envelope. If one assumes that deep mixing (from some nonconvective transport mechanism) was in effect, from the extensive report of Nollett et al. (2003) this would require penetration of a circulating mass to temperatures close to that of the H-burning zone ($\log T \approx 7.7$

K). This is the same as the circulation penetration required for some oxide grains of circumstellar condensates (see Zinner 2014, pp. 181–213). For 3 $M_\odot$ the production of ^{60}Fe is very low, and using the same dilution factor as for ^{182}Hf gives $^{60}\mathrm{Fe}/^{56}\mathrm{Fe} = 5.52 \times 10^{-9}$, far below the upper bound cited above.

The deep mixing needed to produce ^{26}Al is known to be required in the envelopes of low-mass ($\lesssim 2\,M_\odot$) red giant branch stars, as discussed in Section 2. Observational evidence for extra mixing in the envelopes of intermediate-mass stars of $\approx 3\,M_\odot$ is less clear but could come from the high He/H and N/O ratios observed in Type I and bipolar planetary nebulae, which likely evolved from intermediate-mass progenitors $\geqslant 2\,M_\odot$ (Corradi & Schwarz 1995; Karakas et al. 2009). The extra mixing mechanism operating in the envelopes of intermediate-mass stars of $\approx 3\,M_\odot$ is, however, unknown but could be the combination of thermohaline and rotation-induced mixing (e.g., Charbonnel & Lagarde 2010).

There is an issue with regard to the production of ^{26}Al for 4–5.5 $M_\odot$ stars. These are transitional as they lie at the border between no HBB and intense HBB ($M > 6\,M_\odot$). If some penetrative extra mixing process or a stronger HBB could be operative at around 5 $M_\odot$, then one might appeal to that mechanism to make the dilution factors compatible between ^{26}Al and ^{182}Hf, for which case ^{107}Pd will essentially agree with the data. It is also possible that ^{13}C pockets may be operative as an important neutron source (i.e., normal *s*-process). With regard to the low-mass case (3–4 $M_\odot$) it is clear that a self-consistent solution for ^{26}Al, ^{182}Hf, and ^{107}Pd with some form of extra mixing may be possible and gross overproduction of ^{60}Fe avoided, but this would not explain CAIs with fractionation and unidentified nuclear isotope effects showing the initial presence of ^{182}Hf but no ^{26}Al (Holst et al. 2013). Furthermore, the problem remains as to how these lower-mass to intermediate-mass stars with long evolutionary lifetimes could be in molecular clouds with lifetimes of $\approx 10^8$ yr and contribute to the cloud medium.

4. Limitations on the AGB Model Calculations

The conclusions drawn here are limited by uncertainties in the models for the yields of intermediate-mass AGB stars. It is well established that these stars undergo HBB (see recent overview by Ventura & D'Antona 2011). However, the quantitative effect of HBB in stellar models is dependent on how convective mixing is implemented. For the mixing length method used in our models, the temperature at the base of the convective envelope increases with the value of the free mixing length parameter, α_{MLT}. Other mixing schemes produce different results; the Full Spectrum of Turbulence models used by Ventura et al. (2013) result in higher HBB temperatures than we obtain, while the models of Cristallo et al. (2015) present typically lower temperatures for the same mass and metallicity. We expect massive AGB stars to produce ^{26}Al, but we cannot accurately establish at which initial stellar mass HBB may actually start. A problem affecting the production of ^{26}Al by HBB is that the rate of the destruction reaction $^{26}\mathrm{Al}+p$ is uncertain (Siess & Arnould 2008). Thus, an accurate ^{26}Al yield cannot be well established.

The yields of all species are affected by the mass-loss rate. This is because mass loss determines the AGB lifetime and hence the number of TPs, as well as the duration of HBB. Faster mass loss, for example, results in lower yields of ^{26}Al, because there is less time for HBB to operate, and lower yields of ^{60}Fe and ^{182}Hf, because there are fewer TPs and TDU events. In our models, we used the semi-empirical mass-loss prescription by Vassiliadis & Wood (1993). The production of species in the He intershell also depends on the TDU efficiency. This remains a debated uncertainty for intermediate-mass AGB models (Frost & Lattanzio 1996; Mowlavi 1999; Kalirai et al. 2014). Models of massive AGB stars that experience no or little dredge-up (such as the FRUITY model for 6 $M_\odot$; Cristallo et al. 2015) do not present large yields for either ^{60}Fe or ^{182}Hf.

While there are clearly some uncertainties, we feel that some conclusions appear clear. The production of the early solar system inventory of ^{182}Hf from massive AGB stars is inevitably accompanied by production of ^{60}Fe to levels above those inferred to have been present in the early solar system. The presence of a ^{13}C pocket could change this result, since in this case the elements that are produced from Fe seeds (including, e.g., ^{180}Hf and ^{108}Pd) yield high isotopic ratios (e.g., $^{182}\mathrm{Hf}/^{180}\mathrm{Hf}$, $^{107}\mathrm{Pd}/^{108}\mathrm{Pd}$) in the stellar envelope. The elements that are not greatly enhanced by an intrinsic *s*-process (e.g., Ti, Fe, Ni) do not produce high isotopic ratios in the envelope (compare $^{107}\mathrm{Pd}/^{108}\mathrm{Pd}$, $^{182}\mathrm{Hf}/^{180}\mathrm{Hf}$, and $^{60}\mathrm{Fe}/^{56}\mathrm{Fe}$ in Tables 2 and 3). For a case with a ^{13}C pocket, the production of ^{60}Fe can be kept small and that of ^{182}Hf can be large. However, ^{13}C pockets are not expected to be present in AGB stars suffering HBB, both theoretically (Goriely & Siess 2004) and observationally (García-Hernández et al. 2013). This means that a decoupling of ^{182}Hf from ^{60}Fe also gives low ^{26}Al. We see no means of producing ^{182}Hf without high $^{60}\mathrm{Fe}/^{56}\mathrm{Fe}$, unless the current nuclear physics inputs (neutron-capture cross sections of ^{59}Fe and ^{60}Fe, the decay rate of ^{59}Fe, or the rates of the $^{22}\mathrm{Ne}+\alpha$ reactions) are extremely inaccurate.

Thus, even considering the model uncertainties, we do not find a possible self-consistent solution for the origin of ^{26}Al, ^{60}Fe, and ^{182}Hf in the early solar system for initial masses $>6\,M_\odot$.

5. Conclusions

From consideration of the results obtained in the stellar models of Karakas & Lugaro (2016) of intermediate-mass stars and comparing the output of stars ranging in mass from $4M_\odot$ to 8 $M_\odot$, we conclude that the inventory of ^{26}Al, ^{182}Hf, ^{107}Pd, and ^{60}Fe assumed for the early solar system cannot be explained by sources of mass $>6\,M_\odot$. There is a clear need to establish stricter $^{60}\mathrm{Fe}/^{56}\mathrm{Fe}$ values at the times of CAI formation. Sources of lower mass (4–5.5 $M_\odot$), which are transitional in nature, may play a significant role. As HBB is not a dominant feature of these stars, it is possible that the extra mixing processes that produce ^{26}Al and the formation of ^{13}C pockets may permit a possible solution. This would then be similar to models of 2–3 $M_\odot$ AGB stars as sources. The objection to low-mass AGB stars as a source of short-lived nuclei for the solar system is based on the long timescales for evolution to the AGB phase as compared to the lifetime of a molecular cloud ($\sim 10^6$–10^7 yr). The evolutionary timescales for 5.5 and 3 $M_\odot$ stars are ~77 and 650 Myr, respectively. These stars require efficient extra mixing and would not violate the ^{60}Fe bound. It is not evident that the timescales for stellar evolution for such stars are short enough for their contribution to nucleosynthesis in molecular clouds. The association of more massive star formation within molecular clouds is evident from many observations of OB associations. The conclusions drawn here

point to a difficulty in relating the formation of the solar system to such a cloud. One possible solution is that there are always many older stars present within a molecular cloud. These are not, in general, comoving with the cloud, but are passing through it by differential motion. If we consider the volume density of main-sequence stars of $\approx 1\,M_\odot$ in the solar neighborhood to be ~ 1 star parsec^3 and take the size of a cloud to be 30 pc, then the number of stars in the corresponding volume is $\sim 3 \times 10^4$. Using a Salpeter initial mass function, this gives $\sim 10^3$ $3\,M_\odot$ stars in the cloud. This suggests that along the spiral arms of the Galaxy, where the gas is concentrated, longer-lived, lower-mass stars (2–5 $M_\odot$) have a reasonable probability of evolving to planetary nebulae and mixing with clouds, leading to new star formation. A serious answer depends on the appropriate astration rate as a function of stellar mass and the volume density of stars $>1\,M_\odot$ in the spiral arm region where the solar system was hatched.

This work was supported by the Epsilon Foundation (G.J.W.). One of us acknowledges the aid of Anneila Sacajawea Sargent, who guided us to Nick Scoville, who responded to the question, "Could low mass stars from earlier generations be in a molecular cloud?" M.L. is a Momentum ("Lendület-2014" Programme) project leader of the Hungarian Academy of Sciences. A.K. and M.L. warmly thank Yongzhong Qian for his help with revising the manuscript after the passing of Jerry, and thank the referee for comments that have greatly helped to improve the paper.

Appendix A
Issues Concerning ^{26}Al and CAIs

There are three matters concerning ^{26}Al in the CAIs that require attention. The first of these is the presence of CAIs and ultrarefractory oxides with ^{26}Al/^{27}Al ratios ranging from 5×10^{-5} to values some decades below this (see Makide et al. 2011). These samples also have low ^{18}O/^{16}O and ^{17}O/^{16}O ratios, but have ^{17}O/^{18}O of the terrestrial value (e.g., ^{16}O enriched). This oxygen effect in CAIs was first discovered by Clayton et al. (1973). These workers also showed the presence of ^{16}O-depleted material in phases in the same CAIs. This was the result of alteration of O in these phases. Several of these phases also exhibit clear excesses on ^{26}Mg from ^{26}Al decay. Note that some of the phases in CAIs with "oxygen" alteration have the canonical ^{26}Al/^{27}Al ratio. See recent summary by Krot et al. (2014) of the oxygen problem and references therein.

The ^{16}O-enriched oxygen found in phases in CAIs and ultrarefractories is currently believed to represent the actual solar inventory inferred from measurements of the solar wind by the *GENESIS* spacecraft (McKeegan et al. 2011). If the original solar inventory of ^{26}Al/^{27}Al is $\approx 5.5 \times 10^{-5}$, then the CAIs and ultrarefractory grains (such as Al_2O_3) that have "solar" oxygen and ^{26}Al/^{27}Al ranging from $\sim 5 \times 10^{-5}$ to very low values must reflect the passage of time from an initial state or incomplete mixing of stellar debris with no ^{26}Al and with no other detectable nuclear effects (see Makide et al. 2011). It has been proposed that this might result from the very late injection of ^{26}Al into the solar nebula, in which no ^{26}Al was present. This late injection scenario would require that no other nuclear effects would be added and does not explain the well-defined upper bound of ^{26}Al/^{27}Al $= 5.5 \times 10^{-5}$.

Alternatively, the refractories with very low to no ^{26}Al/^{27}Al could represent ongoing infall from the local interstellar medium over a timescale of $\approx 3 \times 10^6$ yr and the solar oxygen then reflecting ongoing infall from that medium. This long-timescale view is in conflict with the typical collapse times of $\sim 10^5$ yr (see Boss 2011). However, it is well known that differential motion of an accreting star through a cloud over 3×10^6 yr can readily provide the last ~3% of a solar mass from ongoing infall due to gravitational sweep-up (Hoyle 1939; Bondi & Hoyle 1944; Edgar 2004; Edgar & Clarke 2004). It is thus reasonable that the range of ^{26}Al/^{27}Al might be due to this process of ongoing late infall from an initial homogeneous source region. This model also implies that the ultrarefractories and CAIs formed over an extended time period and that some had to form by shock heating of infalling debris.

The second issue is the multistage growth of CAIs. It is well known that individual CAIs (~1 cm) are a composite of different material. El Goresy et al. (1985) showed that there are distinct multilayers, and Hsu et al. (2000) showed that layers in a single CAI represent differences of $\sim 10^5$ yr or more using ^{26}Al as a chronometer.

The third and last issue relates to the problem of terrestrial type oxygen, which dominates the "normal"-Fe, Mg-rich chondrules and the terrestrial planets so far sampled. The alteration of oxygen in CAIs (see Krot et al. 2014) and the origin of terrestrial type oxygen are mysteries that are much discussed and little understood by all parties. Many of the phases considered to be primary and to have ^{26}Al/^{27}Al $\approx 5 \times 10^{-5}$ have undergone oxygen exchange by some unknown mechanisms. With these caveats, we consider that the issue of possible stellar sources of ^{26}Al as discussed here is sound.

Appendix B
The Problem of the Initial ^{60}Fe/^{56}Fe

As a guide, we note that the steady-state ratio for the Galaxy based on gamma-ray fluxes from the decay of ^{60}Fe and ^{26}Al are $(^{60}\mathrm{Fe}/^{56}\mathrm{Fe})_{\mathrm{GALS}} = 1.5 \times 10^{-7}$ and $(^{26}\mathrm{Al}/^{27}\mathrm{Al})_{\mathrm{GALS}} = 1.0 \times 10^{-5}$ (Diehl et al. 2010; Diehl 2016). There are no data on ^{60}Fe that can be used from CAIs because (1) widespread isotopic anomalies in both Fe and Ni in CAIs prevent one from obtaining meaningful results on ^{60}Ni, and (2) the Fe in CAIs is not, in general, a primary constituent. Fe is not an ultrarefractory element, and the frequent occurrence of FeS in CAIs is interpreted to reflect late-stage alteration processes that are known to have occurred. With regard to data obtained on planetary differentiates, to be of merit it must be connected to the initial ^{26}Al inventory. For timescales >5 Myr, ^{26}Al has decayed and any connection in time to CAIs is obscure. In any case, as the effects in ^{60}Ni become exceedingly small, the problem of widespread isotopic heterogeneity in the solar system becomes severe.

The required datum is ^{60}Fe/^{56}Fe at the time when ^{26}Al/^{27}Al $\approx 5 \times 10^{-5}$. In attempting to obtain some estimate of this, it has been necessary to analyze Fe and Mg chondrules from unequilibrated ordinary chondrites (UOCs). These chondrules are made of silicates with "terrestrial"-type oxygen. Previous workers have shown that some of these chondrules contain Al-rich phases and exhibit excesses of ^{26}Mg/^{24}Mg correlated with ^{27}Al/^{24}Mg (Hutcheon & Hutchison 1989). Such samples thus may exhibit clear evidence of ^{26}Al and can be related to the CAIs by using the inferred ^{26}Al/^{27}Al ratio as a measure of time. Measurements of ^{60}Fe on samples of chondrules from UOCs and bulk chondrites have yielded a wide range of results. It must be recognized that these measurements are exceedingly difficult. Precise measurements by Tang & Dauphas (2015)

give $^{60}Fe/^{56}Fe \approx 5 \times 10^{-9}$ at the time of crystallization of a chondrule from Semarkona (UEC) and an inferred initial value of $\sim 10^{-8}$. An investigation by Tachibana et al. (2006) gave $^{60}Fe/^{56}Fe \approx (2–4) \times 10^{-7}$ at the time of formation of some chondrules. However, no evidence for the presence of ^{26}Al was obtained in either report. In the study by Mishra & Goswami (2014) measurements were of both Al–Mg and Fe–Ni isotopic systematics on chondrules from some UOC samples. Some of the Al–Mg data were obtained by Rudraswami et al. (2008). We restrict our attention to those samples with rather clear $^{26}Mg/^{24}Mg$–$^{27}Al/^{24}Mg$ correlations, defined $^{26}Al/^{27}Al$ initial values, and a reasonably justified correlation of $^{60}Ni/^{62}Ni$ versus $^{56}Fe/^{62}Ni$. Using the ^{26}Al data as a measure of time, five samples define a value of $(^{60}Fe/^{56}Fe)_{CAI}$ in the range of 5×10^{-7} to 10^{-6} (Mishra & Goswami 2014). It is this data set that is the basis of the upper bound used here. There are no data available that indicate a higher value.

References

Abia, C., Busso, M., Gallino, R., et al. 2001, ApJ, 559, 1117
Abia, C., Domínguez, I., Gallino, R., et al. 2002, ApJ, 579, 817
Angelou, G. C., Stancliffe, R. J., Church, R. P., Lattanzio, J. C., & Smith, G. H. 2012, ApJ, 749, 128
Arnould, M., Goriely, S., & Jorissen, A. 1999, A&A, 347, 572
Asplund, M., Grevesse, N., Sauval, A. J., & Scott, P. 2009, ARA&A, 47, 481
Bloecker, T., & Schoenberner, D. 1991, A&A, 244, L43
Bondarenko, V., Berzins, J., Prokofjevs, P., et al. 2002, NuPhA, 709, 3
Bondi, H., & Hoyle, F. 1944, MNRAS, 104, 273
Boothroyd, A. I., & Sackmann, I.-J. 1992, ApJL, 393, L21
Boothroyd, A. I., Sackmann, I.-J., & Wasserburg, G. J. 1995, ApJL, 442, L21
Boss, A. P. 2011, ApJ, 739, 61
Burkhardt, C., Kleine, T., Bourdon, B., et al. 2008, GeCoA, 72, 6177
Busso, M., Gallino, R., Lambert, D. L., Travaglio, C., & Smith, V. V. 2001, ApJ, 557, 802
Busso, M., Gallino, R., & Wasserburg, G. J. 1999, ARA&A, 37, 239
Charbonnel, C. 1994, A&A, 282, 811
Charbonnel, C., & Lagarde, N. 2010, A&A, 522, A10
Charbonnel, C., & Zahn, J.-P. 2007, A&A, 467, L15
Chen, J. H., & Wasserburg, G. J. 1996, GMS, 95, 1
Clayton, R. N., Grossman, L., & Mayeda, T. K. 1973, Sci, 182, 485
Corradi, R. L. M., & Schwarz, H. E. 1995, A&A, 293, 871
Cristallo, S., Piersanti, L., Straniero, O., et al. 2011, ApJS, 197, 17
Cristallo, S., Straniero, O., Piersanti, L., & Gobrecht, D. 2015, ApJS, 219, 40
Diehl, R. 2016, JPhCS, 665, 012011
Diehl, R., Lang, M. G., Martin, P., et al. 2010, A&A, 522, A51
Doherty, C. L., Gil-Pons, P., Lau, H. H. B., Lattanzio, J. C., & Siess, L. 2014, MNRAS, 437, 195
Duprat, J., & Tatischeff, V. 2007, ApJL, 671, L69
Edgar, R. 2004, NewAR, 48, 843
Edgar, R., & Clarke, C. 2004, MNRAS, 349, 678
Eggleton, P. P., Dearborn, D. S. P., & Lattanzio, J. C. 2008, ApJ, 677, 581
El Goresy, A., Armstrong, J. T., & Wasserburg, G. J. 1985, GeCoA, 49, 2433
Fishlock, C. K., Karakas, A. I., Lugaro, M., & Yong, D. 2014, ApJ, 797, 44
Fitoussi, C., Duprat, J., Tatischeff, V., et al. 2008, PhRvC, 78, 044613
Frost, C. A., & Lattanzio, J. C. 1996, ApJ, 473, 383
Gallino, R., Arlandini, C., Busso, M., et al. 1998, ApJ, 497, 388
García-Hernández, D. A., Zamora, O., Yagüe, A., et al. 2013, A&A, 555, L3
Gilroy, K. K. 1989, ApJ, 347, 835
Gilroy, K. K., & Brown, J. A. 1991, ApJ, 371, 578
Goriely, S., & Siess, L. 2004, A&A, 421, L25
Gounelle, M., Shu, F. H., Shang, H., et al. 2006, ApJ, 640, 1163
Herwig, F. 2005, ARA&A, 43, 435
Holst, J. C., Olsen, M. B., Paton, C., et al. 2013, PNAS, 110, 8819
Horan, M. F., Carlson, R. W., & Blichert-Toft, J. 2012, E&PSL, 351, 215
Hoyle, F. 1939, Obs, 62, 217
Hsu, W., Wasserburg, G. J., & Huss, G. R. 2000, E&PSL, 182, 15
Hutcheon, I. D., & Hutchison, R. 1989, Natur, 337, 238
Iliadis, C., Karakas, A. I., Prantzos, N., Lattanzio, J. C., & Doherty, C. L. 2016, ApJ, 818, 98
Izzard, R. G., Lugaro, M., Karakas, A. I., Iliadis, C., & van Raai, M. 2007, A&A, 466, 641
Kalirai, J. S., Marigo, P., & Tremblay, P.-E. 2014, ApJ, 782, 17
Käppeler, F., Gallino, R., Bisterzo, S., & Aoki, W. 2011, RvMP, 83, 157
Karakas, A. I. 2010, MNRAS, 403, 1413
Karakas, A. I. 2014, MNRAS, 445, 347
Karakas, A. I., García-Hernández, D. A., & Lugaro, M. 2012, ApJ, 751, 8
Karakas, A. I., & Lattanzio, J. C. 2003, PASA, 20, 393
Karakas, A. I., & Lattanzio, J. C. 2007, PASA, 24, 103
Karakas, A. I., & Lattanzio, J. C. 2014, PASA, 31, 30
Karakas, A. I., & Lugaro, M. 2016, ApJ, 825, 26
Karakas, A. I., van Raai, M. A., Lugaro, M., Sterling, N. C., & Dinerstein, H. L. 2009, ApJ, 690, 1130
Krot, A. N., Nagashima, K., Wasserburg, G. J., et al. 2014, GeCoA, 145, 206
Kruijer, T. S., Fischer-Gödde, M., Kleine, T., et al. 2013, E&PSL, 361, 162
Kruijer, T. S., Kleine, T., Fischer-Gödde, M., Burkhardt, C., & Wieler, R. 2014a, E&PSL, 403, 317
Kruijer, T. S., Touboul, M., Fischer-Gödde, M., et al. 2014b, Sci, 6188, 1150
Lattanzio, J. C. 1992, PASA, 10, 120
Limongi, M., & Chieffi, A. 2006, ApJ, 647, 483
Lugaro, M., Heger, A., Osrin, D., et al. 2014, Sci, 345, 650
Lugaro, M., & Karakas, A. I. 2008, NewAR, 52, 416
Lugaro, M., Karakas, A. I., Stancliffe, R. J., & Rijs, C. 2012, ApJ, 747, 2
Makide, K., Nagashima, K., Krot, A. N., et al. 2011, ApJL, 733, L31
Marigo, P., Bressan, A., Nanni, A., Girardi, L., & Pumo, M. L. 2013, MNRAS, 434, 488
Matthes, M., Fischer-Gödde, M., Kruijer, T. S., Leya, I., & Kleine, T. 2015, GeCoA, 169, 45
McKeegan, K. D., Kallio, A. P. A., Heber, V. S., et al. 2011, Sci, 332, 1528
Meyer, B. S. 1994, ARA&A, 32, 153
Mishra, R. K., & Goswami, J. N. 2014, GeCoA, 132, 440
Mowlavi, N. 1999, A&A, 344, 617
Mowlavi, N., & Meynet, G. 2000, A&A, 361, 959
Nollett, K. M., Busso, M., & Wasserburg, G. J. 2003, ApJ, 582, 1036
Palmerini, S., La Cognata, M., Cristallo, S., & Busso, M. 2011, ApJ, 729, 3
Pan, L., Desch, S. J., Scannapieco, E., & Timmes, F. X. 2012, ApJ, 756, 102
Pignatari, M., Herwig, F., Hirschi, R., et al. 2016, ApJS, 225, 24
Rauscher, T., Heger, A., Hoffman, R. D., & Woosley, S. E. 2002, ApJ, 576, 323
Rudraswami, N. G., Goswami, J. N., Chattopadhyay, B., Sengupta, S. K., & Thapliyal, A. P. 2008, E&PSL, 274, 93
Siess, L., & Arnould, M. 2008, A&A, 489, 395
Tachibana, S., Huss, G. R., Kita, N. T., Shimoda, G., & Morishita, Y. 2006, ApJL, 639, L87
Takahashi, K., & Yokoi, K. 1987, ADNDT, 36, 375
Takigawa, A., Miki, J., Tachibana, S., et al. 2008, ApJ, 688, 1382
Tang, H., & Dauphas, N. 2015, ApJ, 802, 22
Trigo-Rodríguez, J. M., García-Hernández, D. A., Lugaro, M., et al. 2009, M&PS, 44, 627
van Raai, M. A., Lugaro, M., Karakas, A. I., & García-Hernández, D. A. 2008, in AIP Conf. Ser. 1001, Evolution and Nucleosynthesis in AGB Stars (Melville, NY: AIP), 146
Vassiliadis, E., & Wood, P. R. 1993, ApJ, 413, 641
Ventura, P., Carini, R., & D'Antona, F. 2011, MNRAS, 415, 3865
Ventura, P., & D'Antona, F. 2005a, A&A, 431, 279
Ventura, P., & D'Antona, F. 2005b, A&A, 439, 1075
Ventura, P., & D'Antona, F. 2011, MNRAS, 410, 2760
Ventura, P., Di Criscienzo, M., Carini, R., & D'Antona, F. 2013, MNRAS, 431, 3642
Ventura, P., Karakas, A. I., Dell'Agli, F., et al. 2015, MNRAS, 450, 3181
Wasserburg, G. J., Busso, M., Gallino, R., & Nollett, K. M. 2006, NuPhA, 777, 5
Wasserburg, G. J., Busso, M., Gallino, R., & Raiteri, C. M. 1994, ApJ, 424, 412
Weiss, A., & Ferguson, J. W. 2009, A&A, 508, 1343
Woosley, S. E., & Weaver, T. A. 1995, ApJS, 101, 181
Zinner, E. 2014, in Microphysics of Cosmic Plasmas, ed. A. M. Davis (Amsterdam: Elsevier)